Sustainable Energy & Fuels

ROYAL SOCIETY OF CHEMISTRY

PAPER

View Article Online
View Journal | View Issue

Cite this: *Sustainable Energy Fuels*, 2025, **9**, 4894

Ferromagnetic–antiferromagnetic interfaces in MAX phase electrocatalysts: a spin-driven platform for enhanced oxygen evolution reaction

Deepak Vishnu S. K.,†[abc] Chih-Ying Huang,†[ad] Cheng-Rong Wu,[e] Bo-Yan Lin,[f] Chia-Chun Chen,[f] Huang-Ming Tsai,[g] Jau-Wern Chiou,[h] Raman Sankar,*[i] Tsyr-Yan Yu,*[acd] Chi-Kung Ni,*[bc] Way-Faung Pong[j] and Chun-Wei Chen*[dek]

The oxygen evolution reaction (OER) is limited by high activation barriers and sluggish kinetics, constraining the efficiency of water electrolysis. Spin-polarized electrons on catalyst surfaces are crucial for generating parallel spin-aligned oxygen, thereby enhancing OER performance. This study introduces a novel electrocatalyst system using a ferromagnetic (FM) MAX phase to improve spin-enhanced OER activity. Through isomorphous replacement, we synthesized the Ti_2FeN (TFN) MAX phase with excess iron toppling onto its surface (T-TFN). Unlike the pristine TFN with a Curie temperature (T_C) of 208 K, T-TFN exhibits room-temperature ferromagnetism, with a T_C exceeding 300 K. When paired with non-FM Co_3O_4 nanoparticles, the T-TFN/Co_3O_4 hybrid system demonstrates significantly enhanced OER activity under an external magnetic field. The FM ordering in T-TFN induces spin alignment at the TFN/Co_3O_4 interface *via* the spin-pinning effect, reducing electron–electron repulsion and facilitating efficient charge transfer. This synergy of high conductivity and room-temperature ferromagnetism in T-TFN creates an effective platform for magnetic field-assisted electrocatalysis. The hybrid system highlights the potential of FM MAX phases as a catalyst support, paving the way for more efficient OER and advancements in water-splitting technologies.

Received 3rd June 2025
Accepted 28th July 2025

DOI: 10.1039/d5se00780a

rsc.li/sustainable-energy

Introduction

The existing energy supply is largely dependent on fossil fuel combustion, which results in considerable greenhouse gas emissions that jeopardize the environment.[1] Consequently, it is vital to explore alternative energy sources and reduce carbon emissions. Electrocatalytic water splitting for the production of clean hydrogen is a promising approach to address this significant issue and has been extensively researched over the past decade.[2,3] As the counter half-reaction, the oxygen evolution reaction (OER), which involves four-electron transfer and exhibits sluggish kinetics, is considered a bottleneck for overall performance.[4] To design high-efficiency catalysts, commonly reported strategies include enhancing the intrinsic activity and increasing the number of active sites in the catalysts.[2,5,6] Recently, the manipulation of electronic spin has emerged as a promising strategy to boost the performance of OER catalysts.[7–9] In the OER process, the formation of a dioxygen bond must adhere to the principle of spin conservation from quantum mechanics, which states that the total spin of a system remains unchanged unless influenced by an external force. This principle is crucial for the generation of paramagnetic (PM) triplet-state oxygen, which has a lower reaction barrier compared to singlet-state oxygen, where electrons have opposite spins.[10] Spin-polarized electrons on the catalyst surface play a crucial role in promoting the generation of parallel spin-aligned oxygen, thereby enhancing the performance of the OER. The OER activity of FM catalysts, such as the metal oxides $NiZnFe_4O_x$ and $CoFe_2O_4$, can be significantly enhanced by applying an external magnetic field.[11] By contrast, antiferromagnetic (AFM) and PM catalysts do not show any improvement in OER activity when exposed to an external magnetic field.[12]

[a]*Molecular Science and Technology Program, Taiwan International Graduate Program (TIGP), Academia Sinica, Taipei, 11529, Taiwan*
[b]*Department of Chemistry, National Tsing Hua University, Hsinchu 30013, Taiwan*
[c]*Institute of Atomic and Molecular Sciences, Academia Sinica, Taipei 10617, Taiwan. E-mail: tyyu@pub.iams.sinica.edu.tw; ckni@po.iams.sinica.edu.tw*
[d]*International Graduate Program of Molecular Science and Technology (NTU-MST), National Taiwan University, Taipei 10617, Taiwan. E-mail: chunwei@ntu.edu.tw*
[e]*Department of Materials Science and Engineering, National Taiwan University, Taipei 10617, Taiwan*
[f]*Department of Chemistry, National Taiwan Normal University, Taipei 11677, Taiwan*
[g]*National Synchrotron Radiation Research Center, Hsinchu 300, Taiwan*
[h]*Department of Applied Physics, National University of Kaohsiung, Kaohsiung 811, Taiwan*
[i]*Institute of Physics, Academia Sinica, Taipei 115201, Taiwan. E-mail: sankarraman@as.edu.tw*
[j]*Department of Physics, Tamkang University, New Taipei City 251301, Taiwan*
[k]*Center for Condensed Matter Sciences and Center of Atomic Initiative for New Materials (AI-MAT), National Taiwan University, Taipei 10617, Taiwan*
† These authors contributed equally.

This phenomenon is further corroborated by theoretical simulations demonstrating that FM catalysts exhibit improved OER activity due to quantum spin exchange interactions (QSEI), which reduce electronic repulsion in magnetic systems.[13,14] Furthermore, several studies suggest that FM catalysts exhibiting a spin-pinning effect at the FM/oxyhydroxide interface could significantly enhance the spin-dependent kinetics of the OER.[15] The interfacial coupling between FM and AFM phases serves as a spin filter in core–shell catalysts, selectively extracting electrons that have spins opposite to the magnetic moment of the FM core during the oxygen evolution reaction.[16] Accordingly, even when FM oxides are coated with a PM hydroxide layer resulting from surface reconstruction, the OER performance still significantly improves under the influence of an external magnetic field due to the spin pinning effect.[15]

Two-dimensional (2D) transition metal carbides and nitrides, referred to as MXenes, have gained significant attention for their potential in energy conversion and storage applications.[17] Although intrinsic MXenes do not demonstrate promising catalytic activity, they are recognized as effective supports for co-catalysts, owing to their high conductivity, surface hydrophilicity, and excellent electrochemical stability.[18] Numerous catalysts, including noble metals,[19] metal oxides,[20] layered double hydroxides,[21] metal–organic frameworks,[22] and graphitic carbon nitride (g-C_3N_4),[23] have been combined with MXenes to form hybrid structures, yielding significantly enhanced catalytic performances. MXenes, which have a general formula of $M_{n+1}X_nT_x$ (M is an early transition metal, X is C or N or both, and T_x is surface termination groups), are typically produced by the top-down separation from their parent layered MAX ($M_{n+1}AX_n$) phases (where A is 13–16 groups, $n = 1$–3).[24] MAX phases are a group of naturally nano-laminated ternary carbides and nitrides characterized by a hexagonal crystal lattice. MAX phases consist of a single-atom-thick layer of A atoms, featuring weak interactions between the A atoms and neighboring M atoms.[25] These unique properties enable the substitution of the A layer with magnetic elements such as Fe, Co, or Ni, thereby introducing FM characteristics to the material. Although synthesizing ferromagnetic MXenes remains a significant challenge, FM MAX phases have recently been successfully produced. Recently, Li *et al.* employed MAX phases as a scaffold to synthesize various ferromagnetic MAX phases by substituting the non-magnetic aluminum (Al) layers with Fe atoms, exhibiting near-room temperature FM behaviors.[26]

The aim of this work is to synthesize the room-temperature FM MAX phase as an effective catalyst support to enhance electrocatalytic OER. In this study, we synthesized Ti_2FeN (TFN) and a variant with an iron topping on Ti_2FeN, designated as T-TFN. The Curie temperature (T_C) increases from 208 K for the pristine TFN MAX phase to above room temperature for the T-TFN, enabling the latter to exhibit ferromagnetism at room temperature. When combined with the non-FM Co_3O_4 nanoparticle cocatalyst, this FM MAX phase hybrid system exhibits promising OER activity when exposed to an external magnetic field, outperforming the non-FM MAX phase counterpart. This approach aims to utilize the room-temperature ferromagnetism of T-TFN as a promising support platform to enhance the magnetically assisted OER for non-FM catalysts, similar to the spin pinning effect. The magnetic properties of the FM MAX phase T-TFN were also investigated using advanced characterization techniques, including superconducting quantum interference device (SQUID), X-ray magnetic circular dichroism (XMCD), and electron paramagnetic resonance (EPR), which confirmed the fundamental FM behavior at room temperature. Combining the advantages of high conductivity and room temperature ferromagnetism of T-TFN, our results pave the way for designing efficient catalysts for OER through magnetic field-assisted electrocatalysis by utilizing FM MAX phase materials as a promising support platform.

Results and discussions

The TAN MAX phase was initially synthesized using a high-temperature arc melting technique, ensuring high purity and quality of the sample using X-ray diffraction (XRD). The Al interlayer in the TAN structure was then replaced with Fe, resulting in the formation of two distinct Fe-based MAX phases, TFN and T-TFN, through an isomorphous replacement reaction. $FeCl_2$ was used as the Lewis salt to facilitate the substitution process, as detailed in the SI (Fig. S1).[26] Fig. 1(a) shows

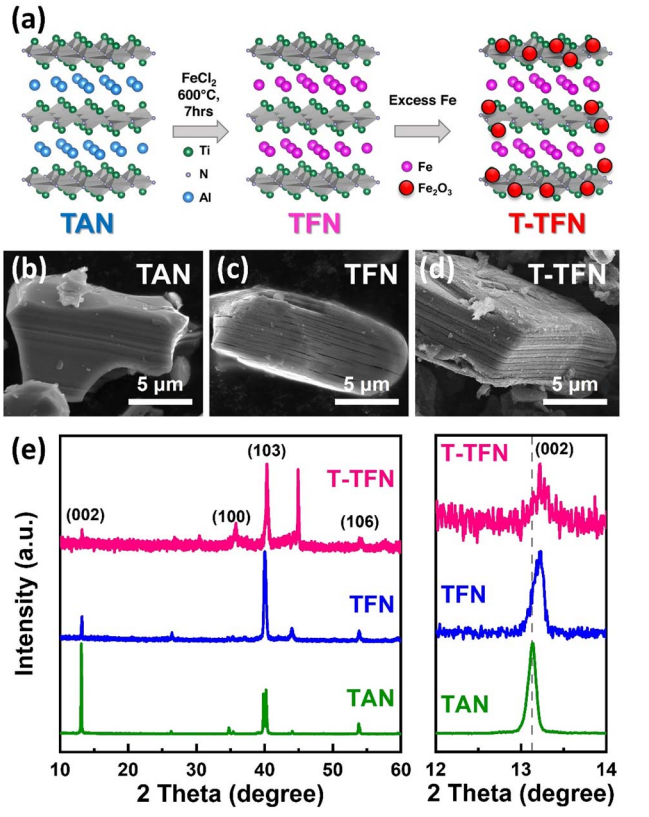

Fig. 1 (a) The schematic diagram of the synthesis process for MAX phase Ti_2AlN (TAN), the sequential effect after Al substitution by Fe (TFN), and excess Fe toppling on TFN surface (T-TFN); (b) the modifications on the surface observed by SEM images on the TAN, (c) TFN, and (d) T-TFN; (e) XRD patterns of the TAN, TFN and T-TFN, respectively.

the schematic diagram of the synthesis process for the TAN, TFN, and T-TFN MAX phases, which exhibit a hexagonal crystal structure belonging to the $P6_3/mmc$ space group. In the TFN MAX phase, Al atoms in TAN were substituted with Fe, preserving the structural integrity while introducing FM behavior. The materials TAN and TFN feature a distinctive two-dimensional nanolaminate architecture composed of alternating layers of titanium nitride (Ti_6N) and Al or Fe. The Al or Fe layers located between the Ti–N layers have metallic characteristics and are weakly bonded, exhibiting exceptional electrical conductivity, thermal resistance, and mechanical robustness.[27] In the isomorphous replacement reaction, atomically thin aluminum was replaced with iron through the use of $FeCl_2$. During this process, excess iron deposited on the surface leads to the formation of T-TFN. Subsequent washing with 3 M HCl removes the excess surface iron, resulting in the formation of TFN. In the T-TFN phase, excess Fe was added not only to replace Al but also to be deposited on the surface, resulting in increased Fe content and enhanced FM properties compared to TFN. This modification of the MAX phase structure is crucial to developing materials that combine high conductivity and room temperature ferromagnetism for magnetically assisted OER, as detailed in the following section.

The corresponding scanning electron microscopy (SEM) images of TAN, TFN, and T-TFN MAX phases are shown in Fig. 1(b–d), where TAN and TFN exhibit a similar layered structure as shown in Fig. 1(b and c). By contrast, Fig. 1(d) shows the presence of excess Fe toppled on the surface of T-TFN. The excess Fe in the T-TFN MAX phase was partially oxidized corresponding to Fe_2O_3, which will be further confirmed by the XMCD measurement in the next section. The X-ray diffraction (XRD) analysis of the synthesized TAN, TFN, and T-TFN MAX phases produced *via* an isomorphous replacement approach is shown in Fig. 1(e). The replacement of Al atoms with Fe in these phases results in no significant changes to the overall crystal structure, as indicated by the similarity in the XRD patterns of the modified and original MAX phases. Additionally, the appearance of an extra peak around 45° in the XRD pattern of T-TFN is attributed to the presence of excess Fe deposited on the surface of TFN.[28,29] Zoom in on the peak of the (002) plane from 12° to 14°. It shows a slight peak shift to a higher degree is due to the Fe atom substitution. High-resolution transmission electron microscopy (HRTEM) images provide additional insights to confirm lattice modifications. The interlayer distance of TAN is 0.230 nm, which is slightly smaller than those of TFN and T-TFN (0.232 nm), as shown in Fig. S2, aligning with the (103) planes of the MAX phases.[30]

The magnetic properties of TAN, TFN, and T-TFN were systematically measured using SQUID magnetometry and vibrating sample magnetometry (VSM) to understand the transition from ferromagnetism to paramagnetism as a function of temperature. Fig. 2(a and b) illustrate this transition, where a decrease in magnetization is observed as the temperature increases, which is characteristic of the transition from FM to PM phases. Both Fe-based MAX phases of TFN and T-TFN exhibit ferromagnetism, but the T_C of the two materials differs. As indicated by the zero-field-cooled magnetization

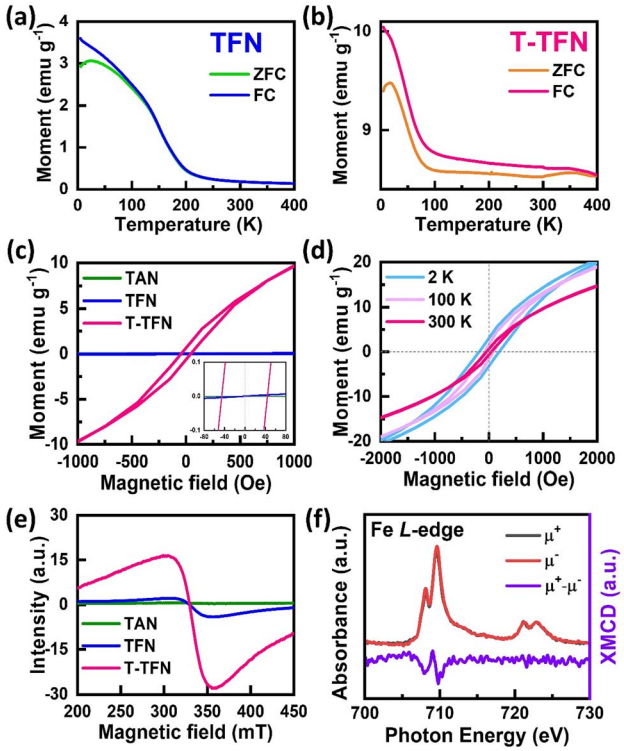

Fig. 2 Temperature dependence of ZFC and FC magnetization curves for the MAX phases (a) TFN and (b) T-TFN. (c) Magnetic hysteresis loops at 300 K of TAN, TFN, and T-TFN. (d) Field-dependent magnetization curves of T-TFN at different temperatures. (e) EPR spectra of TAN, TFN, and T-TFN at room temperature. (f) XMCD spectra of T-TFN at room temperature, circularly right polarized (μ^+), circularly left polarized (μ^-), and their difference ($\mu^+ - \mu^-$).

curves, T-TFN exhibits FM behavior with a T_C exceeding room temperature, while TFN exhibits similar FM properties but with a T_C of 208 K, observed below room temperature. This suggests that T-TFN, with its T_C above room temperature, could be suitable for applications that require room-temperature FM properties, such as magnetically enhanced OER. These magnetic properties are further evidenced in Fig. 2(c), which presents isothermal magnetic measurements taken at room temperature. T-TFN shows a hysteresis loop at 300 K, indicative of its FM nature, while both TAN and TFN do not exhibit such behavior, confirming the absence of magnetic ordering in these materials at room temperature. Fig. 2(d) exhibits the temperature-dependent magnetic hysteresis loops of T-TFN measured from 2–300 K. The room-temperature FM behavior of T-TFN can be further confirmed by the EPR and XMCD measurements at room temperature, as shown in Fig. 2(e and f), respectively. The observed EPR spectrum is mainly due to the presence of unpaired electrons in the materials. There is no EPR signal for the TAN sample. TFN exhibits only a slight signal, while T-TFN displays a significantly stronger signal. This suggests that the additional iron oxide on the surface of T-TFN likely introduces more unpaired electrons, leading to a stronger EPR signal compared to TFN.[31] XMCD measurements were also performed at room temperature to investigate the origin of

ferromagnetism in T-TFN. The corresponding X-ray absorbance spectrum (XAS) and XMCD spectrum are shown in Fig. 2(f). In the Fe $L_{3,2}$-edge XAS spectrum, circular right-polarized and circular left-polarized light is denoted as μ^+ and μ^-, respectively. The L_3 peak appears at approximately 709.6 eV, while the L_2 peak is observed around 721.1 eV, both originating from Fe_2O_3.[32,33] Notable changes in the difference spectrum ($\mu^+ - \mu^-$) of XMCD are located in the corresponding L_3 region. The XMCD peaks display the characteristic electronic structure of Fe^{3+}, which is attributed to the t_{2g}–e_g splitting in octahedral sites. This phenomenon is associated with the contribution of the magnetic moment from the $2p_{3/2}$ electrons in Fe.[34] Additionally, the edge position of the XAS suggests that Fe predominantly exists in the oxidized state, with its energy at the $L_{3,2}$-edge being similar to that of Fe_2O_3.[35] As seen in Fig. 2(d), the hysteresis loops become more pronounced when the temperature decreases, which is attributed to the strong FM coupling among oxidized Fe ions within the T-TFN system. This broadening of the hysteresis curve reflects the enhanced FM properties at lower temperatures, primarily resulting from the magnetic moments of Fe-oxide (Fe_2O_3). The presence of excess Fe_2O_3 leads to strong FM coupling within the T-TFN system, as evidenced by the magnetic hysteresis, coercivity measurements, and temperature-dependent magnetization behavior. The result suggests that the FM T-TFN, with its T_C above room temperature, could be applicable in electrochemical applications, particularly in magnetically enhanced OER. In addition, the XPS spectra of Ti 2p, Al 2p, N 2s, and Fe 2p in TAN and T-TFN are shown in Fig. S4. The spectra show characteristic peaks of the TAN MAX phase comparable with the previous reports.[40,41] It's clear to see that most of the Al 2p spectrum were replaced by the Fe 2p spectrum as seen from the XPS spectra of TAN and T-TFN in Fig. S5. The Fe 2p spectrum suggests that Fe undergoes oxidation from the T-TFN surface, consistent with the XMCD spectra in Fig. 2(f).

It is widely known that although the pristine MXenes and MAX phases possess high conductivity and surface area, they often exhibit slow water oxidation kinetics.[36] By contrast, these materials can effectively act as catalyst supports, immobilizing catalyst particles to develop efficient OER catalysts.[37] Many reports have demonstrated the coupling of MXene support with catalysts, such as CoP, CoS_2, and FeNi-LDH, to facilitate OER.[36,38,39] Because T-TFN combines both the advantages of high conductivity and ferromagnetism at room temperature, it may serve as a promising support candidate for magnetically assisted OER. Here, the FM T-TFN MAX phase functions as a catalyst support, coupling with the OER-active catalyst Co_3O_4 to form a co-catalyst system. The FM T-TFN is decorated with Co_3O_4 using a hydrothermal method to form the T-TFN/Co_3O_4 hybrid, which enables magnetically assisted OER. Fig. 3(a) exhibits the SEM image of Co_3O_4 nanoflakes grown on the surface of T-TFN, while elemental mapping from EDX analysis reveals a uniform distribution of Ti, Fe, and Co. The SEM image and EDX mapping of the TAN/Co_3O_4 catalyst are shown in Fig. S3. The XRD patterns confirm the presence of Co_3O_4 within the T-TFN and TAN structures, as shown in Fig. S6. The HRTEM image of the T-TFN/Co_3O_4 hybrid shows the (111) plane of Co_3O_4 and the (103) plane of T-TFN, with corresponding *d*-spacings of 0.463 nm and 0.232 nm as illustrated in Fig. 3(b). Fig. S7 shows the Raman spectra of T-TFN, T-TFN/Co_3O_4, and Co_3O_4. The Raman peak at 600 cm^{-1} comes from the active modes of the rutile phase and the peak located at ~450 cm^{-1} is related to the oxide phase. It is evident that T-TFN/Co_3O_4 exhibits a peak at approximately 700 cm^{-1}, which originates from Co_3O_4 and is consistent with previous reports.[42,43] The result supports the coexistence of both the Co_3O_4 catalyst and FM T-TFN MAX phase in the T-TFN/Co_3O_4 hybrid system.

The OER performance of T-TFN/Co_3O_4 was evaluated using a conventional three-electrode system in 1.0 M KOH, with the results of linear sweep voltammetry (LSV) shown in Fig. 3(c). For comparison, the OER performances of the non-FM MAX phase TAN/Co_3O_4 hybrid system and the individual catalysts of TAN, T-TFN, and Co_3O_4 were also measured. Co_3O_4 exhibits an overpotential of 450 mV to achieve a current density of 10 mA cm^{-2}, consistent with other reports in the literature.[44–46] Neither T-TFN nor TAN showed any electrocatalytic activity toward OER, similar to the reported result in the literature.[47,48] By contrast, a significant enhancement in the OER catalytic activity can be seen in both TAN/Co_3O_4 and T-TFN/Co_3O_4 hybrids, mainly arising from the synergistic effect between the conductive MAX phase and the active sites provided by Co_3O_4. Both TAN/Co_3O_4 and T-TFN/Co_3O_4 hybrids exhibit an improved OER catalytic activity with an overpotential of 390 mV (at 10 mA cm^{-2}) compared to the pristine Co_3O_4. As shown in Fig. 3(d), the Tafel slope analysis indicates improved reaction kinetics for TAN/Co_3O_4 and T-TFN/Co_3O_4, with slopes of 107 mV dec^{-1} and 99 mV dec^{-1}, respectively—both notably lower than that of pristine Co_3O_4 (152 mV dec^{-1}). The reduction in Tafel slope values after the incorporation of the MAX phases TAN and T-TFN with Co_3O_4 indicates their influential role as catalyst supports in enhancing kinetic activities, attributed to their high conductivity. Electrochemical impedance spectroscopy (EIS) was employed to evaluate the charge transfer resistance (R_{ct}) during the OER process, as illustrated in Fig. 3(e). Nyquist plots were analyzed using the Randles equivalent circuit model, comprising resistance at the electrolyte–catalyst interface, capacitance, and charge-transfer resistance at the electrolyte–electrode interface.[49] The fitted semicircles indicated a significant reduction in R_{ct} from 86 Ω for Co_3O_4 to 33 Ω for T-TFN/Co_3O_4, highlighting excellent charge transfer efficiency when incorporating the MAX phase support. The corresponding overpotentials, Tafel slopes, and charge transfer resistances for all MAX phases, Co_3O_4, TAN/Co_3O_4, and T-TFN/Co_3O_4 hybrids are detailed in Table S1. Chronoamperometry was conducted to evaluate the long-term stability of T-TFN/Co_3O_4 and TAN/Co_3O_4 at a potential of 1.7 V *vs.* RHE. Both hybrid materials exhibited stable performance, maintaining 90% of their initial currents over a 72-hour duration, as shown in Fig. 3(f), indicating their excellent stability for OER applications in alkaline environments. Additionally, the LSV curves obtained after the stability assessment demonstrated consistent performance throughout the 72-hour reaction period (Fig. S8). Furthermore, the electrochemical active surface area (ECSA) among these catalysts were assessed by cyclic voltammetry with different scan

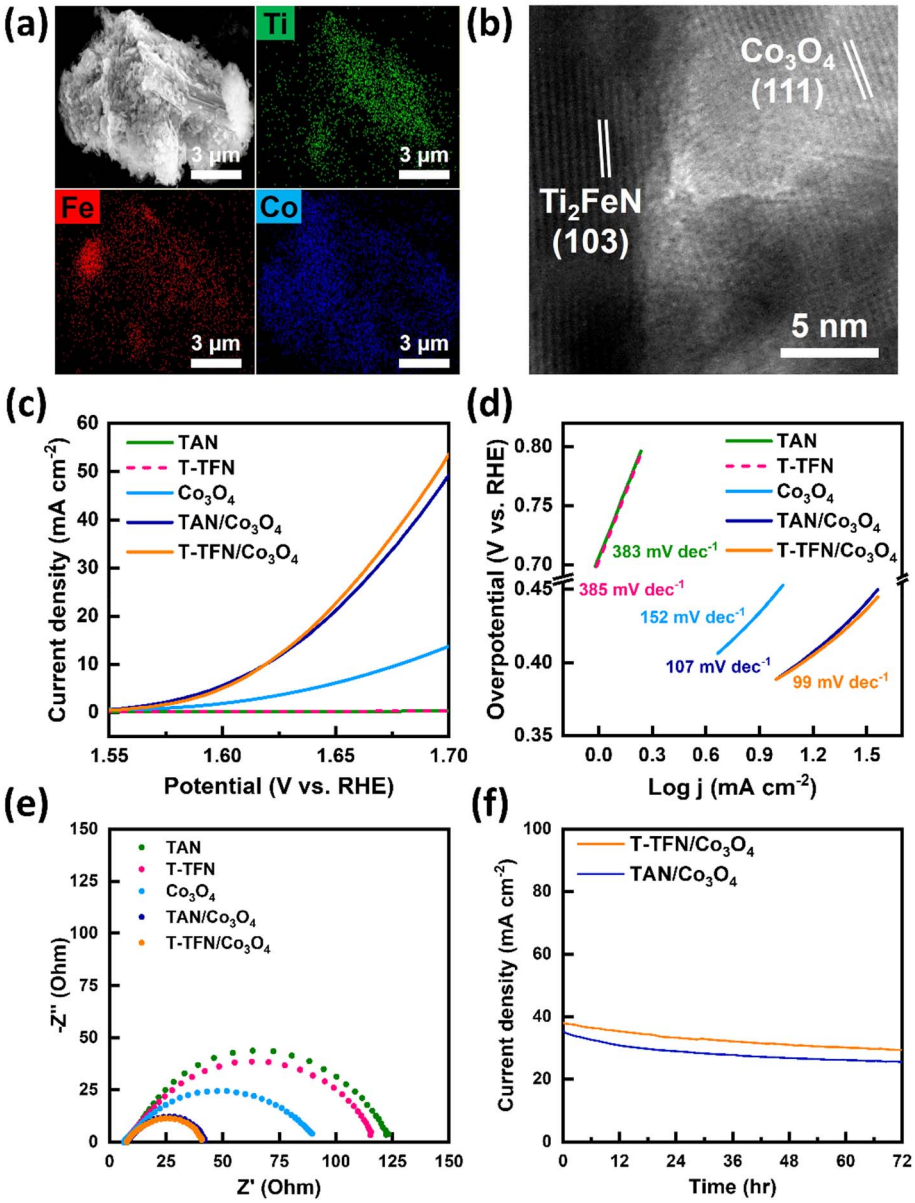

Fig. 3 (a) SEM micrograph and its corresponding EDX mapping of the T-TFN/Co_3O_4 catalyst. (b) HRTEM image of T-TFN/Co_3O_4. (c) *iR*-Corrected LSV curves in 1 M $KOH_{(aq)}$. (d) Corresponding Tafel plots of TAN, T-TFN, Co_3O_4, TAN/Co_3O_4, and T-TFN/Co_3O_4. (e) Electrochemical impedance spectroscopy (EIS) of pure TAN, T-TFN, Co_3O_4, TAN/Co_3O_4, and T-TFN/Co_3O_4, respectively. (f) Chronoamperometric OER stability assessment through controlled potential electrolysis was conducted at an applied potential of 1.7 V (*vs.* RHE) in 1 M KOH electrolyte for TAN/Co_3O_4 and T-TFN/Co_3O_4, respectively.

rates in a non-faradaic region, as shown in Fig. S9. The ECSA results of TAN/Co_3O_4 and T-TFN/Co_3O_4 are similar, excluding the variations in active surface areas among different catalyst systems. The LSV curves further normalized by the ECSA of these catalysts are shown in Fig. S10.

Next, the magnetic field-enhanced OER performances for the T-TFN/Co_3O_4 and TAN/Co_3O_4 hybrids were measured by applying the permanent magnets to the three-electrode system. The magnetic field-enhanced OER performances of TAN/Co_3O_4 and T-TFN/Co_3O_4 with and without an external magnetic field of 0.3 T are shown in Fig. 4(a). Although the overpotential of T-TFN/Co_3O_4 decreases modestly by 20 mV (from 390 to 370 mV at 10 mA cm^{-2}) under a magnetic field of 0.3 T, the corresponding current density exhibits a significant enhancement. The comparison of OER performance of MAX phase and MXene catalysts was shown in Table S2. The current density at 1.65 V *vs.* RHE increases by nearly 98%, underscoring the strong catalytic promotion induced by the magnetic field. This significant current enhancement indicates a marked improvement in charge transfer kinetics and highlights the critical role of spin alignment in accelerating the OER process. By contrast, the effect of the magnetic field on the OER performance is also examined by investigating the TAN/Co_3O_4 electrochemical behavior under the same magnetic field conditions. The LSV

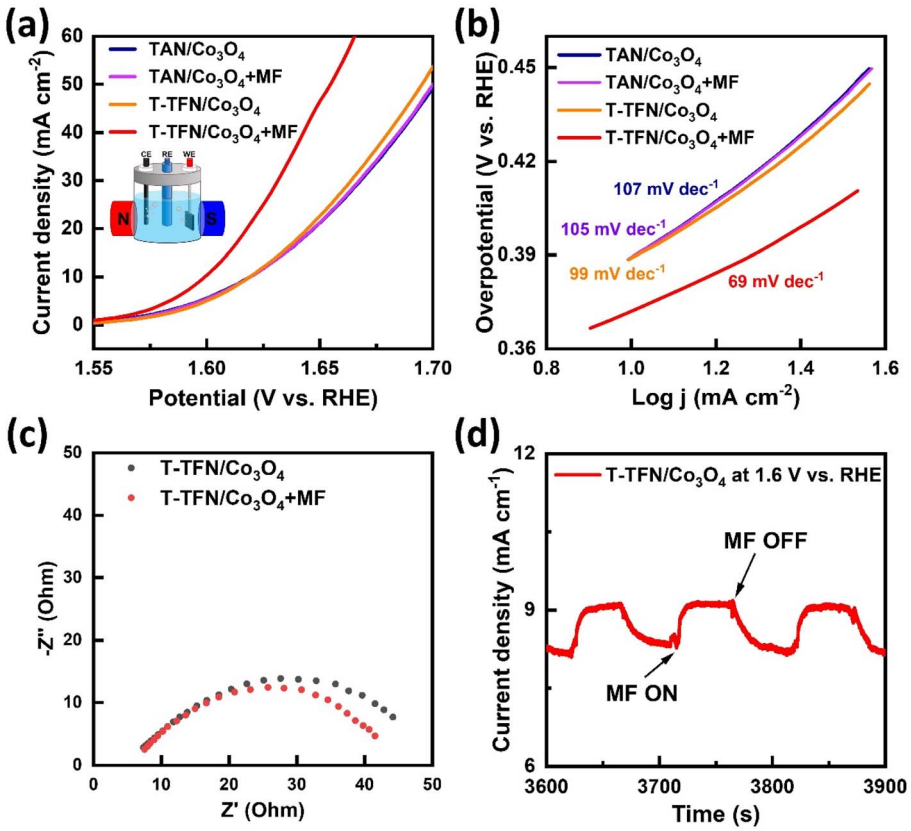

Fig. 4 (a) *iR*-Corrected LSV curves of TAN/Co_3O_4 and T-TFN/Co_3O_4 with and without external magnetic field (MF), inset shows the illustration of magnetic field enhanced electrocatalysis setup, and (b) corresponding Tafel plots. (c) EIS of T-TFN/Co_3O_4 with and without MF. (d) Pulsed magneto chronoamperometric of T-TFN/Co_3O_4 at a constant potential of 1.6 V *vs.* RHE after 1 hour stabilized.

curves exhibit no discernible impact on the OER performances with and without an external magnetic field. Fig. 4(b) shows the corresponding Tafel slopes for the OER performances of the TAN/Co_3O_4 and T-TFN/Co_3O_4 hybrids under an external magnetic field. Since Co_3O_4 is classified as an AFM material, the above results suggest that the enhanced OER performance of the T-TFN/Co_3O_4 hybrid under an external magnetic field is primarily attributed to the FM behavior of T-TFN. By contrast, no such enhancement is observed for the non-FM behavior of TAN. Fig. 4(c) shows the reduction in the R_{ct} values of the T-TFN/Co_3O_4 hybrid after applying an external magnetic field by the EIS measurement. Fig. 4(d) displays the *i*–*t* curve of T-TFN/Co_3O_4 under magnetic field switching after 1 hour stabilized, demonstrating a consistent electrocatalytic response under the influence of a magnetic field. The above results suggest that coupling the FM T-TFN MAX phase support with the non-FM Co_3O_4 catalyst makes magnetically assisted OER feasible when an external magnetic field is applied.

The magnetic field-enhanced OER in the FM T-TFN/Co_3O_4 hybrid can be attributed to the spin pinning effect at the FM/non-FM interface.[15,16,50] As illustrated in Fig. S11, the FM T-TFN induces spin alignment in adjacent non-FM Co_3O_4, enabling spin-polarized electron transfer. According to QSEI theory,[14] aligned spins reduce electron–electron repulsion during intermediate adsorption, enhancing charge transport.[12] Specifically, in the rate-determining $O^* + OH^- \rightarrow OOH^* + e^-$ step,[51] spin alignment of OH^- minimizes repulsion and promotes electron transfer. Under a magnetic field, FM ordering in T-TFN strengthens, aligning spins across the interface and enabling efficient triplet oxygen formation from singlet OH^- reactants.[15,16,50] This spin-pinned interface lowers energy barriers, accelerating reaction kinetics. Thus, the T-TFN's high conductivity and room-temperature ferromagnetism offer an effective platform for magnetic field-assisted OER catalysis, even with non-FM Co_3O_4.

Conclusions

In conclusion, we have synthesized FM MAX phase-derived T-TFN and T-TFN/Co_3O_4 hybrid structures to realize the magnetically enhanced OER. Combining the advantages of high conductivity and room-temperature ferromagnetism of T-TFN, T-TFN/Co_3O_4 exhibits promising magnetic enhancement in OER under an external magnetic field. The T-TFN MAX phase functions as an excellent catalyst support platform for integrating with other non-FM catalysts for OER. This integration not only enhances their performance through magnetic field-assisted electrocatalysis but also opens up new avenues for designing advanced catalytic systems.

Conflicts of interest

There are no conflicts to declare.

Data availability

The data supporting this article have been included as part of the SI.

Experimental sections, characterization methods, and other electrocatalytic analysis. See DOI: **https://doi.org/10.1039/d5se00780a**.

Acknowledgements

C.-W. C. acknowledges the financial support from the National Science and Technology Council (NSTC), Taiwan (Grant No. NSTC-109-2124-M-002-002-MY3, 111-2124-M-002-021, 110-2113-M-002-019-MY3, 112-2124-M-011-001, 112-2119-M-A49-012-MBK, 112-2813-C-002-007-M). Financial support by the Center of Atomic Initiative for New Materials (AI-MAT), National Taiwan University, from the Featured Areas Research Center Program within the framework of the Higher Education Sprout Project by the Ministry of Education in Taiwan (Grant No. 111L900801), is also acknowledged. R. S. acknowledges NSTC, Taiwan (Grant No. NSTC-113-2124-M-001-003 and NSTC-113-2112-M-001-045-MY3). The Fe $L_{3,2}$-edge XAS and XMCD spectra obtained from beamline Taiwan Photon Source (TPS) 45A2 at the National Synchrotron Radiation Research Center (NSRRC) are appreciated.

References

1 F. Johnsson, J. Kjärstad and J. Rootzén, The threat to climate change mitigation posed by the abundance of fossil fuels, *Clim. Policy*, 2019, **19**(2), 258–274.
2 Z. W. Seh, *et al.*, Combining theory and experiment in electrocatalysis: Insights into materials design, *Science*, 2017, **355**(6321), eaad4998.
3 J. Zhu, *et al.*, Recent advances in electrocatalytic hydrogen evolution using nanoparticles, *Chem. Rev.*, 2019, **120**(2), 851–918.
4 W. Zhang, *et al.*, Progress and perspective of electrocatalytic CO_2 reduction for renewable carbonaceous fuels and chemicals, *Adv. Sci.*, 2018, **5**(1), 1700275.
5 W. T. Hong, *et al.*, Toward the rational design of non-precious transition metal oxides for oxygen electrocatalysis, *Energy Environ. Sci.*, 2015, **8**(5), 1404–1427.
6 J. Song, *et al.*, A review on fundamentals for designing oxygen evolution electrocatalysts, *Chem. Soc. Rev.*, 2020, **49**(7), 2196–2214.
7 G. Zhou, *et al.*, Spin-state reconfiguration induced by alternating magnetic field for efficient oxygen evolution reaction, *Nat. Commun.*, 2021, **12**(1), 4827.
8 A. Vadakkayil, *et al.*, Chiral electrocatalysts eclipse water splitting metrics through spin control, *Nat. Commun.*, 2023, **14**(1), 1067.
9 Z. Fang, *et al.*, Spin-modulated oxygen electrocatalysis, *Precis. Chem.*, 2023, **1**(7), 395–417.
10 Y. Sun, *et al.*, Spin-related electron transfer and orbital interactions in oxygen electrocatalysis, *Adv. Mater.*, 2020, **32**(39), 2003297.
11 F. A. Garcés-Pineda, *et al.*, Direct magnetic enhancement of electrocatalytic water oxidation in alkaline media, *Nat. Energy*, 2019, **4**(6), 519–525.
12 X. Ren, *et al.*, Spin-polarized oxygen evolution reaction under magnetic field, *Nat. Commun.*, 2021, **12**(1), 2608.
13 L. Zhang, *et al.*, Ferromagnetic ligand holes in cobalt perovskite electrocatalysts as an essential factor for high activity towards oxygen evolution, *Phys. Chem. Chem. Phys.*, 2019, **21**(6), 2977–2983.
14 C. Biz, M. Fianchini and J. Gracia, Strongly correlated electrons in catalysis: focus on quantum exchange, *ACS Catal.*, 2021, **11**(22), 14249–14261.
15 T. Wu, *et al.*, Spin pinning effect to reconstructed oxyhydroxide layer on ferromagnetic oxides for enhanced water oxidation, *Nat. Commun.*, 2021, **12**(1), 3634.
16 J. Ge, *et al.*, Ferromagnetic–antiferromagnetic coupling core–shell nanoparticles with spin conservation for water oxidation, *Adv. Mater.*, 2021, **33**(42), 2101091.
17 N. K. Chaudhari, *et al.*, MXene: an emerging two-dimensional material for future energy conversion and storage applications, *J. Mater. Chem. A*, 2017, **5**(47), 24564–24579.
18 J. Lee, *et al.*, Design Strategies of Active and Stable Oxygen Evolution Catalysts for Proton Exchange Membrane Water Electrolysis, *Energy Fuels*, 2023, **37**(23), 17736–17753.
19 J. Zhang, *et al.*, Single platinum atoms immobilized on an MXene as an efficient catalyst for the hydrogen evolution reaction, *Nat. Catal.*, 2018, **1**(12), 985–992.
20 D. Tyndall, *et al.*, Understanding the effect of MXene in a TMO/MXene hybrid catalyst for the oxygen evolution reaction, *npj 2D Mater. Appl.*, 2023, **7**(1), 15.
21 J. Wang, *et al.*, Subtle 2D/2D MXene-Based Heterostructures for High-Performance Electrocatalytic Water Splitting, *Small Methods*, 2024, 2301602.
22 A. Hanan, *et al.*, MOFs coupled transition metals, graphene, and MXenes: Emerging electrocatalysts for hydrogen evolution reaction, *Chem. Eng. J.*, 2024, 148776.
23 W. Liu, *et al.*, Ti_3C_2 MXene embellished g-C_3N_4 nanosheets for improving photocatalytic redox capacity, *J. Alloys Compd.*, 2021, **877**, 160223.
24 Y. Gogotsi and Q. Huang, MXenes: Two-Dimensional Building Blocks for Future Materials and Devices, *ACS Nano*, 2021, **15**(4), 5775–5780.
25 H. Fashandi, *et al.*, Ti_2Au_2C and $Ti_3Au_2C_2$ formed by solid state reaction of gold with Ti_2AlC and Ti_3AlC_2, *Chem. Commun.*, 2017, **53**(69), 9554–9557.
26 Y. Li, *et al.*, Near-room temperature ferromagnetic behavior of single-atom-thick 2D iron in nanolaminated ternary MAX phases, *Appl. Phys. Rev.*, 2021, **8**(3), 031418.
27 M. W. Barsoum, The $M_{N+1}AX_N$ phases: A new class of solids: Thermodynamically stable nanolaminates, *Prog. Solid State Chem.*, 2000, **28**(1–4), 201–281.

28 H. D. Omar, To investigation the structure and morphology of iron metallic by difference techniques, *J. Nanotechnol. Adv. Mater.*, 2015, **3**(2), 57–61.
29 P. Zhang, *et al.*, Twin structure of the lath martensite in low carbon steel, *Prog. Nat. Sci.: Mater. Int.*, 2016, **26**(2), 169–172.
30 T. Zhang, *et al.*, Syntheses and properties of Ti_2AlN MAX-phase films, *J. Ceram. Process. Res.*, 2012, **13**(S1), 149–153.
31 I. R. Macdonald, *et al.*, Photoinduced superparamagnetism in nanostructured α-Fe_2O_3, *J. Phys. Chem. Lett.*, 2010, **1**(16), 2488–2492.
32 F. Jiménez-Villacorta, *et al.*, X-ray magnetic circular dichroism study of the blocking process in nanostructured iron-iron oxide core-shell systems, *Phys. Rev. B: Condens. Matter Mater. Phys.*, 2011, **84**(17), 172404.
33 O. Dmitrieva, *et al.*, Magnetic moment of Fe in oxide-free FePt nanoparticles, *Phys. Rev. B: Condens. Matter Mater. Phys.*, 2007, **76**(6), 064414.
34 G. Rossi, *et al.*, Magnetic dichroism in the angular distribution of Fe 2p and 3p photoelectrons: Empirical support to Zeeman-like analysis, *Phys. Rev. B: Condens. Matter Mater. Phys.*, 1997, **55**(17), 11488.
35 N. Kubitza, *et al.*, Microwave-Assisted Synthesis of the New Solid-Solution $(V_{1-x}Cr_x)_2GaC$ $(0 \leq x \leq 1)$, a Pauli Paramagnet Almost Matching the Stoner Criterion for $x = 0.80$, *Chem. Mater.*, 2023, **35**(11), 4427–4434.
36 M. Yu, *et al.*, Boosting electrocatalytic oxygen evolution by synergistically coupling layered double hydroxide with MXene, *Nano Energy*, 2018, **44**, 181–190.
37 S. G. Peera, *et al.*, MXene ($Ti_3C_2T_x$) supported electrocatalysts for methanol and ethanol electrooxidation: A review, *Ceram. Int.*, 2021, **47**(20), 28106–28121.
38 H. Zong, *et al.*, Ultrathin Ti_2NT_x MXene-wrapped MOF-derived CoP frameworks towards hydrogen evolution and water oxidation, *Electrochim. Acta*, 2021, **393**, 139068.
39 S. Han, *et al.*, Multi-dimensional hierarchical CoS_2@MXene as trifunctional electrocatalysts for zinc-air batteries and overall water splitting, *Sci. China Mater.*, 2021, **64**, 1127–1138.
40 Z. Zhang, *et al.*, Oxidation of Single Crystalline Ti_2AlN Thin Films between 300 and 900 °C: A Perspective from Surface Analysis, *J. Phys. Chem. C*, 2016, **120**(33), 18520–18528.
41 N. F. Rosli, *et al.*, MAX and MAB Phases: Two-Dimensional Layered Carbide and Boride Nanomaterials for Electrochemical Applications, *ACS Appl. Nano Mater.*, 2019, **2**(9), 6010–6021.
42 Z. Mahmoudi, *et al.*, Synthesis of Ti_2AlC & Ti_3AlC_2 MAX phases by Arc-PVD using Ti–Al target in C_2H_2/Ar gas mixture and subsequent annealing, *Ceram. Int.*, 2020, **46**(4), 4968–4975.
43 B. Rivas-Murias and V. Salgueiriño, Thermodynamic CoO–Co_3O_4 crossover using Raman spectroscopy in magnetic octahedron-shaped nanocrystals, *J. Raman Spectrosc.*, 2017, **48**(6), 837–841.
44 S. L. Zhang, *et al.*, Metal atom-doped Co_3O_4 hierarchical nanoplates for electrocatalytic oxygen evolution, *Adv. Mater.*, 2020, **32**(31), 2002235.
45 L. Zeng, *et al.*, General approach of in situ etching and doping to synthesize a nickel-doped M_xO_y (M = Co, Mn, Fe) nanosheets array on nickel foam as large-sized electrodes for overall water splitting, *ACS Appl. Energy Mater.*, 2018, **1**(11), 6279–6287.
46 S. Raj, *et al.*, In situ Mn-doping-promoted conversion of $Co(OH)_2$ to Co_3O_4 as an active electrocatalyst for oxygen evolution reaction, *ACS Sustain. Chem. Eng.*, 2019, **7**(10), 9690–9698.
47 M. Khazaei, *et al.*, Insights into exfoliation possibility of MAX phases to MXenes, *Phys. Chem. Chem. Phys.*, 2018, **20**(13), 8579–8592.
48 K. A. Kumar, O. Alduhaish and M. Pumera, Electrocatalytic activity of layered MAX phases for the hydrogen evolution reaction, *Electrochem. Commun.*, 2021, **125**, 106977.
49 S. Wang, *et al.*, Electrochemical impedance spectroscopy, *Nat. Rev. Methods Primers*, 2021, **1**(1), 41.
50 R. R. Chen, *et al.*, $SmCo_5$ with a reconstructed oxyhydroxide surface for spin-selective water oxidation at elevated temperature, *Angew. Chem., Int. Ed.*, 2021, **60**(49), 25884–25890.
51 J. Li, *et al.*, Spin effect on oxygen electrocatalysis, *Adv. Energy Sustainability Res.*, 2021, **2**(8), 2100034.